The Role of Initial Conditions in the Decay of Spatially Periodic Patterns in a Nematic Liquid Crystal

Werner Pesch and Lorenz Kramer

Institute of Physics, University of Bayreuth, D-95440 Bayreuth, Germany

Nándor Éber* and Ágnes Buka

Research Institute for Solid State Physics and Optics,

Hungarian Academy of Sciences, H-1525 Budapest, P.O.B.49, Hungary

(Dated: December 15, 2005)

Abstract

The decay of stripe patterns in planarly aligned nematic liquid crystals has been studied experimentally and theoretically. The initial patterns have been generated by the electrohydrodynamic instability. Light diffraction technique has been used to monitor the relaxation process of the stripe pattern. The theoretical analysis focuses on the one hand on the rigorous determination of the contribution from the individual decay modes to the overall relaxation process of a given initial pattern. On the other hand a refined physical optical description of the diffraction intensity is also given. Controlled modifications of the initial conditions have allowed to assess different decay modes.

PACS numbers: ??? 47.54.+r, 61.30.Gd, 47.20.Ky, 47.20.Lz, 78.20.Jq ???

*Electronic address: eber@szfki.hu

I. INTRODUCTION

The intriguing features of patterns in anisotropic fluids when driven out of equilibrium by an external stress have motivated a wide range of experimental and theoretical studies over the last decades [1]. The most common representatives of uniaxially symmetric fluids are nematic liquid crystals (nematics) which have a locally preferred direction described by the director field $\mathbf{n}(\mathbf{r}, t)$.

One of the simplest examples of patterns in nematics is a regular sequence of parallel dark and bright stripes of wavevector $\mathbf{q}$, which reflect a periodic modulation of the director and hence that of the optical axis in space. The pattern is often accompanied by material flow in the form of convection rolls and can be induced by various types of excitations like shear flow, temperature gradient or electric field.

The goal of this work is to investigate the decay of a suitably prepared uniform stripe pattern after the driving force has been switched off, i.e. when the system is returning to the equilibrium (usually homogeneous) ground state. The relaxation time τ characterizing the decay process is a key parameter, which reflects the system dynamics. In the theoretical analysis we concentrate on low-amplitude director modulations, either already realized in the initial pattern or developing in the late stage of the decay process. In a recent paper [2] a rigorous theoretical description of the low-amplitude decay process of stripes has been presented, which is based on the standard equation set of nematohydrodynamics [3, 4]. One arrives at a certain linear eigenvalue problem, which yields an infinite discrete spectrum of decay rates, $\mu_i(q)$ associated with the corresponding eigen (decay) modes $N_i(z, q)$. Since only the pattern wavelength ($\Lambda = 2\pi/q$) and the elastic and viscous material parameters come into play, the analysis of the decay process might also be useful for actually assessing parameter values. Note that the mechanism of producing the patterns influences their subsequent decay only via the initial conditions, which determine the selection of the relevant decay modes.

In our case electroconvection (EC) is used to trigger the initial patterns: an ac voltage is applied to a thin ($d \sim 10-100\mu$m) layer of a planarly oriented, slightly conducting nematic possessing negative dielectric and positive conductivity anisotropies [5]. Varying the easily tunable control parameters (rms voltage U, circular frequency ω, etc.) we place the system into a parameter regime, where periodic stripe (roll) patterns with wavevector $\mathbf{q}$ parallel to the equilibrium director orientation $\mathbf{n}_0$ (normal rolls) bifurcate at onset (U_c). This state serves as the initial condition for the decay dynamics when the voltage is switched off. Our previous light diffraction measurements of the decay rates for various $|\mathbf{q}|$ were consistent with the theory and gave the first indications to the selection mechanism of the dominant decay modes [2]. In the present work the analysis will be substantially refined: for a given initial pattern we determine rigorously the individual contributions of the different decay modes to the temporal evolution of the diffraction fringe intensities, which is exploited in the experiment to monitor the decay process.

In Section II we describe briefly the experimental setup and give some background information on the initial EC patterns. Section III is devoted to the linear eigenvalue problem alluded to before, which leads to the decay rate spectrum and in particular to the understanding of the relative importance of the corresponding eigenmodes when the decay from different initial states is considered. In Section IV we present a theoretical analysis of the light diffraction method, where we employ a standard (slightly refined) physical optical description [10, 11]. In Section V we compare theory and experiment in the linear regime. In addition we show experiments where the initial conditions have been modified either by stronger forcing or by different waveforms of the driving signal. The paper ends with some concluding remarks and an outlook for future work. An appendix is devoted to some technical details.

II. EXPERIMENTAL SETUP

The decay of EC patterns was investigated in standard sandwich cells (E.H.C. Co) which produce by their proper surface treatment a uniform planar orientation of nematics in the equilibrium state. In the experiments we have used the commercial nematic 'Phase 5' (Merck) and its factory doped version `Phase 5A`. This substance (a kind of a standard for EC measurements) is chemically stable and its material parameters on which all explicit calculations throughout this paper were based, are well known [6]. All measurements were carried out at the temperature $T = 30.0 \pm 0.05\ {}^{o}$C kept constant by a PC controlled Instec hot-stage. Cells with different thicknesses d have been used, where d was determined by an Ocean Optics spectrophotometer.

The EC instability was typically driven by an ac voltage $U\sqrt{2} sin\omega t$ with frequencies $f = \omega/(2\pi)$ up to 1400 Hz and rms amplitudes U up to 90 V [7]. Convection in form

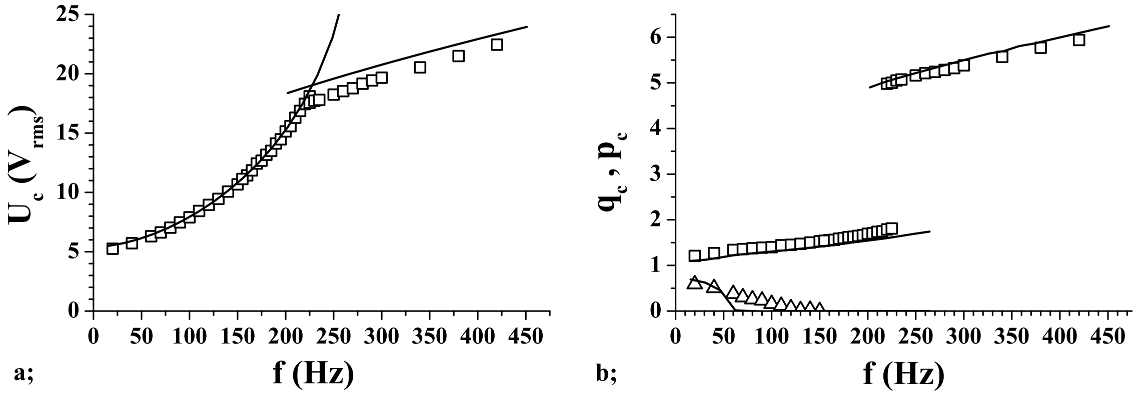

FIG. 1: a; Critical voltage U_c and b; dimensionless components $q'_c = q_c d/\pi$ (open squares) and $p'_c = p_c d/\pi$ (open triangles) of the critical wavevector for a `Phase 5` cell ($d = 9.2\mu$m) as function of frequency f. Measurements (symbols) are compared with theory (solid lines).

of rolls with a critical wavevector $\mathbf{q_c} = (q_c, p_c)$ sets in if the applied voltage U exceeds a certain threshold $U_c(f)$. In Fig. 1a a typical critical voltage curve is presented as a function of frequency, where two well known regimes can clearly be identified. At frequencies below a certain cutoff frequency, f_c, which is material parameter dependent, one observes electroconvection in the *conductive* regime, where the director distortion is practically time independent, whereas it oscillates in the *dielectric* regime above f_c (for more details see Sect.III). The transition from one regime to the other is indicated by a sudden change in the slope of the $U_c(f)$ curve. In Fig. 1b we show the components q, p of the critical wavevector $\mathbf{q}_c$. At lower frequencies we have *oblique* rolls with a nonzero angle $\delta = arctan(p/q)$ between $\mathbf{q}$ and $\mathbf{n}_0$. Above the Lifshitz frequency f_L we have normal rolls with $p_c = 0$. At f_c we observe a jump in q_c. In Figs. 1a and 1b we have included the theoretical curves obtained from the linear stability analysis of the nematohydrodynamic equations [5] with the material parameter set for `Phase 5`, which describes the experiments very well.

The cut-off frequency is proportional to the electric conductivity of a nematic. `Phase 5` has a low cut-off frequency ($f_c = \omega_c/(2\pi) < 300$ Hz) thus it allows easy measurements in the dielectric mode of EC in thin cells. Due to its much higher electrical conductivity `Phase 5A` has a higher cut-off ($f_c > 1500$ Hz) offering a wide frequency range for the conductive mode. But the dielectric regime was not accesible, since the required voltage becomes too high and destroys the cells. To facilitate comparison with theory we restricted ourselves to

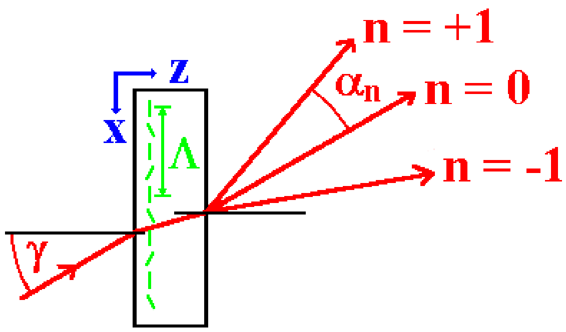

FIG. 2: Schematic sketch of the light diffraction geometry.

the normal roll regime ($f > f_L$). While the wavelength $\Lambda = 2\pi/q$ in the conductive regime varies roughly between $2d$ and $0.9d$, in the dielectric regime considerably smaller values $\approx 0.3d$ become accessible. In order to cover a wide $q-$range we have chosen $d = 28\mu$m for `Phase 5A` and $d = 9.2\mu$m for `Phase 5`, respectively.

The nematic layer (see Fig.2) is illuminated with a polarized monochromatic laser beam (circular frequency Ω, wavelength $\lambda = 2\pi c/\Omega = 650$nm, c is the velocity of light). Diffraction fringes were observed on a screen placed normal to the beam at a distance of $L = 660$ mm. In order to have a higher contrast, oblique incidence was used with an angle of incidence $\gamma = 5^\circ$. This set-up allowed easy determination of the pattern wavelength Λ from the distances of the fringes.

The pattern decay has been initiated by a practically instantaneous (within 10μs) shutting down of the voltage. The process has been monitored by recording the intensity $I_{-1}(t)$ of the first order fringe $n = -1$ [8]. From the analysis of the time evolution of $I_{-1}(t)$, to be described in the subsequent sections, the decay rates could be extracted.

III. THEORETICAL ANALYSIS OF THE DECAY PROCESS

We consider the standard configuration of a nematic sandwiched between two plates parallel to the x-y plane at a distance d ($-d/2 < z < d/2$). We concentrate on the planar configuration, where in the ground state the director is oriented along the x axis, i. e. parallel to $\mathbf{n}_0 = (1, 0, 0)$. Applying an electric voltage U, which exceeds slightly the threshold U_c, a stripe pattern develops. It involves a periodic modulation of $\mathbf{n}$ with wavenumber q in the $\mathbf{n}_0$

direction. The modulations are coupled in a positive feedback to the flow in convection rolls and to space charge distributions with the same periodicity; all spatial variations are confined to the x-z plane (”normal rolls”). $\mathbf{n}$ is characterized by its space- and time dependent angle, $\theta^{EC}(x,z,t)$, with $\hat{\boldsymbol{x}}$. It is convenient to separate an amplitude θ_m and the part periodic along x from θ^{EC}, which is thus presented as $\theta^{EC}(x,z,t) = \theta_m sin(qx)\vartheta^{EC}(q,z,t)$ where $\vartheta^{EC}(q,0,0)$ is normalized to one.

The threshold voltage U_c, the critical wavenumber q_c of the roll pattern and the director profile $\vartheta^{EC}(q,z,t)$ can be obtained from a linear stability analysis of the standard model (SM) of EC [12], which consists of a set of coupled partial differential equations (PDE). Galerkin methods [9] are very convenient to obtain numerical solutions of the SM. The various fields (director, flow, charge density) are represented in the form of appropriate series expansions, like

$$\vartheta^{EC}(q,z,t) = \sum_{m=-\infty}^{\infty} e^{im\omega t} \sum_{l=1}^{\infty} a_{ml}(q) sin(l\frac{\pi}{d}(z+d/2)), \qquad (1)$$

for the director, which automatically fulfill the boundary conditions of vanishing distortion, $\vartheta^{EC}(q,\pm d/2,t) = 0$, at the confining plates. Due to the up-down symmetry of standard EC the solutions are either odd or even against the reflection $z \to -z$. At small dimensionless control parameter values $\epsilon = (V^2 - V_c^2)/V_c^2$, i.e. near onset, ϑ^{EC} is in fact even in z and thus $a_{ml}(q) = 0$ for all even values of l. The solutions are in addition characterized by a parity under the transformation $t \Rightarrow t + \pi/\omega$. While ϑ^{EC} has even parity ($a_{ml} = 0$ for odd m) in the *conductive* regime, it switches to odd parity at the cut-off frequency ω_c for the high-frequency *dielectric* regime ($a_{ml} = 0$ for even m). By projecting the SM equations on the Galerkin modes one arrives at algebraic equations for the expansion coefficients like the $a_{ml}(q)$, which are determined numerically. Truncating at 8 Galerkin modes ($0 < l < 8$) in the $z-$direction and at 3 temporal modes ($0 < |m| < 3$) usually gives an excellent description of patterns near onset. For the nematic `Phase 5` the director profile $\vartheta^{EC}(q,z,t)$ turns out to be dominated by the leading non-vanishing terms ($l = 1; m = 0$ for conductive and $l = 1; m = \pm 1$ for dielectric regimes), while the other coefficients a_{ml} yield only small (< 5 %) corrections.

The decay of a pattern, which starts when the voltage is suddenly switched off, say at $t = 0$, does not change the wavenumber q. Therefore we use for the director profile θ^d during the decay the representation $\theta^d(x,z,t) = \theta_m sin(qx)\vartheta^d(q,z,t)$ in analogy to $\theta^{EC}(x,z,t)$.

As already mentioned the analysis of the decay process requires the solution of a linear eigenvalue problem, which originates from the standard model, to determine the decay rates $\mu_k(q)$ and the decay modes $N_k(q,z)$. Compared to the analogous calculation of the critical EC values, the equations become simpler [2], since for zero electric field the charge and the director relaxation dynamics are decoupled (see Appendix).

In line with the standard procedure for linear PDEs the time evolution of the decaying director profile $\vartheta^d(q,z,t)$ can be represented as:

$$\vartheta^d(q,z,t) = \sum_{k=1}^{\infty} e^{-\mu_k(q)t} w_k(q) N_k(q,z). \tag{2}$$

The expansion coefficients $w_k(q)$ are determined by a suitable projection on the initial state $\vartheta^d(q,z,0) \equiv \vartheta^{EC}(q,z,0)$.

$$w_k(q) = \int_{-d/2}^{+d/2} \vartheta^{EC}(q,z,0) N_k^+(q,z) dz \qquad k = 1,2,... \tag{3}$$

where the adjoint linear eigenvectors $N_k^+(q,z)$ of the eigenvalue problem (see Appendix) fulfill the ortho-normality condition:

$$\frac{1}{d}\int_{-d/2}^{+d/2} N_k(q,z) N_l^+(q,z) dz = \delta_{kl} \qquad k,l = 1,2. \tag{4}$$

where δ_{kl} denotes the Kronecker symbol.

The expansion coefficients $w_k(q)$ depend strongly on q. This is obvious when inspecting the $q-$dependence of the weights w_k $(k = 1,...,8)$ plotted as function of the dimensionless wavenumber square $q'^2 = (qd/\pi)^2$ in Figs. 3a and 3b. The w_k have been determined with the help of Eq. (3), where for simplicity $\vartheta^{EC}(q,z,0)$ has been approximated by its leading term $sin(\frac{\pi}{d}(z+d/2))$ in Eq. (1). The functions $w_k(q)$ are very small everywhere except over a certain q'^2 interval, where they rise steeply to a finite value. In other words the q'^2 axis can be covered by a set of intervals, such that for each of them a unique $\hat{k}(q)$ exists associated with the dominating $w_{\hat{k}}(q)$ function. With increasing q'^2 the corresponding $\hat{k}(q)$ increases monotonously. Only in the vicinity of special q'^2 values, where two neighboring $w_k(q)$ curves cross, i.e at the borders of the q'^2 intervals described before, the decay is governed by two comparable decay rates $\mu_{\hat{k}}$ and $\mu_{\hat{k}+1}$.

We have in addition calculated the weights $w_k(q)$ for some q values using the rigorous theoretical initial director profilea $\vartheta^{EC}(q,z,0)$ in Eq.(3), which includes nonzero coefficients

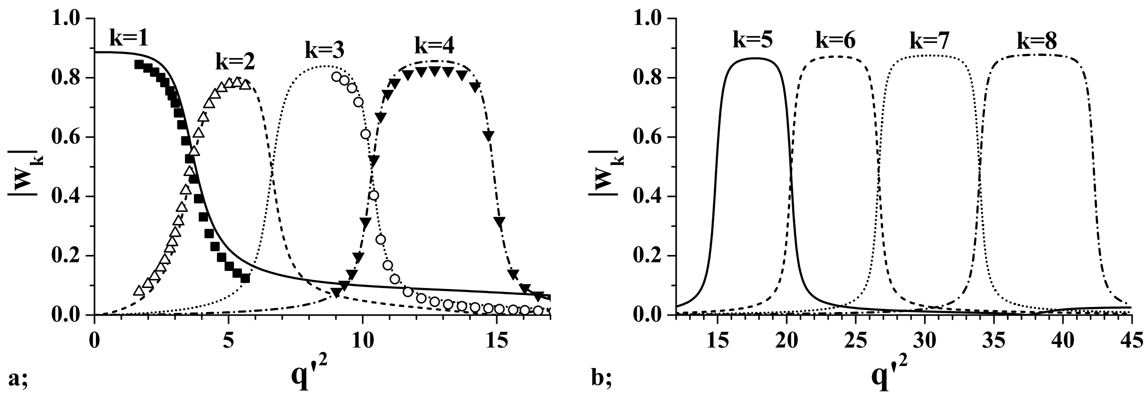

FIG. 3: Variation of the absolute value of the weights w_k of various decay eigenmodes (plotted with different line styles) with respect to the dimensionless wavenumber square q'^2 for a; $k = 1, ..., 4$ and for b; $k = 5, ..., 8$, using a $sin(\frac{\pi}{d}(z + d/2))$ initial director profile. The weights $|w_k|$ calculated from the actual EC director profile are plotted as symbols for a few frequencies in the conductive ($q'^2 < 6$, squares for $k = 1$, up triangles for $k = 2$) as well as in the dielectric regime ($q'^2 > 8$) (circles for $k = 3$ and down triangles for $k = 4$).

a_{ml} with $l > 1$ in Eq. (1). The corrections are in fact almost negligible (see the symbols in Fig. 3a).

IV. THEORETICAL DESCRIPTION OF THE DIFFRACTION OPTICS

EC roll patterns represent a periodic spatial modulation of the director which corresponds to an optical phase grating with a lattice constant Λ. This feature allows us to keep track of the decay of the pattern by monitoring the intensities of the fringes in laser diffraction. Since our director distortions are small, the linearized physical optics approach discussed in the literature for diffraction from EC rolls [10] is well suited. To disentangle clearly the main contributions to the fringe intensities and to set our notation, we review briefly the previous theoretical approach ([10]) and allow at the same time for arbitrary profiles $\vartheta^d(z)$ instead of $\sin[\frac{\pi}{d}(z + d/2)]$ chosen in Ref. [10].

The incident light can be well described by a plane wave $\sim \exp[i(\Omega t - \boldsymbol{k}_0 \boldsymbol{x})]$, since the spatial extension of the beam is much larger than Λ. The wave vector $\boldsymbol{k}_0$ ($k_0 = \Omega/c$) and the (extraordinary) light polarization are restricted to the x-z plane.

The optical properties of the nematic are governed by the anisotropic dielectric permittivities $\epsilon_\parallel, \epsilon_\perp$ (at the optical frequency ω) or by the corresponding refractive indices, $n_e^2 = \epsilon_\parallel, n_o^2 = \epsilon_\perp$.

In the case of small distortions of the planar geometry, i.e. for small θ_m, the diffraction pattern is determined only by the phase $k_0\Phi$ of the transmitted light. Thus an eikonal type approximation for the electric and magnetic field components of the light wave is appropriate. According to [10] in the present geometry the Maxwell equations can be reduced to an equation for the y component of the magnetic field, $\mathbf{B}_y$, of the laser beam. The equation is solved by the substitution:

$$B_y(x,z) = C\exp[i(\omega t + k_0\Phi)] \;\text{ with }\; \Phi(x,z) = x\sin\gamma - n_f z + \beta\theta_m u(x,z). \tag{5}$$

Here C is a constant and the following abbreviations are used :

$$n_f = n_e\sqrt{1 - \frac{\sin^2\gamma}{n_o^2}}, \quad \beta = \frac{n_e^2}{n_o^2} - 1. \tag{6}$$

Obviously the function $u(x,z)$ describes the modification of a plane wave due to the presence of the periodic director distortion.

Following [10] it is useful to separate $u(x,z)$ as

$$u(x,z) = g_1(z)\exp[-iqx] + g_2(z)\exp[iqx] \tag{7}$$

which eventually leads to a linear inhomogeneous ordinary differential equation (ODE) for $g_1(z)$:

$$\begin{aligned}(-\frac{n_e^2}{n_o^2}q^2 + \partial_{zz})g_1(z) - 2ik_0[n_f\partial_z g_1(z) + \frac{n_e^2}{i}q\sin\gamma\; g_1(z)] \\ = [-2k_0 n_f\sin\gamma\;\vartheta(z) - i\sin\gamma\;\partial_z\vartheta(z) + qn_f\vartheta(z)]/2\end{aligned} \tag{8}$$

The corresponding ODE for $g_2(z)$ is obtained by the replacement $q \to -q$.

The standard matching conditions of the light wave at the boundaries of the cell at $z = \pm d/2$ are fulfilled if the following conditions hold [10].

$$g_1(-d/2) = \partial_z g_1(-d/2) = 0; \quad g_2(-d/2) = \partial_z g_2(-d/2) = 0. \tag{9}$$

The maxima of the diffraction patterns correspond to rays which include the angles $\gamma+\alpha_n$ ($n = \pm1,\ \pm2,\ ...$) with the z axis, fulfilling the relation

$$\sin(\gamma + \alpha_n) - \sin(\gamma) = \frac{n\lambda}{\Lambda} \tag{10}$$

where $\alpha_n < 0$ for negative n. In this paper we concentrate on the intensity I_{-1} of the first order fringe $n = -1$ (see Fig. 2). It can be shown by expanding Eq. (5) with respect to $\theta_m \ll 1$ (see [11]), that within our linear approximation scheme I_{-1} is given as $\theta_m^2 |ik_0 g_1(d/2)|^2 := \theta_m^2 |H_1|^2$, where the intensity I_0 of the undistorted laser beam is normalized to one.

We solve Eq. (8) using the '*variation of constant*' method. The two linearly independent solutions of the homogeneous equation are given as $f_{\pm}(z) = \exp(i\kappa_{\pm} z)$ with

$$\kappa_{\pm} = n_f k_0 \left[1 \pm \left(1 - R^{-2} \frac{n_e^2}{n_o^2} [1 - 2R \sin\gamma]/n_f^2 \right)^{1/2} \right]; \quad R = k_0/q. \tag{11}$$

Corrections to geometrical optics and thus diffraction become smaller with increasing R, which varies between 6 and 38 in our experiments. It is obvious, that even a small incidence angle like $\gamma = 5^0$ is advantageous, since the term $2R\sin\gamma$ compensates to some extent the small factor R^{-2} in Eq.(11).

The solution of Eq. (8) with the boundary conditions Eq. (9) is then determined as:

$$g_1(z) = \frac{1}{i(\kappa_+ - \kappa_-)} \int_{-d/2}^{z} dz' \left(f_+(z - z') - f_-(z - z') \right) Inh(z') \tag{12}$$

where $Inh(z)$ denotes the inhomogeneity on the right hand side of the ODE in Eq. (8). It is obvious that the contribution from $f_+(z)$ - which oscillates strongly on the scale of d due to $\kappa_+ \gg \kappa_-$ - can be safely neglected in the sequel.

Thus we arrive at the following final expression for $I_{-1} \propto |H_1|^2$:

$$H_1 = -(\bar{c}_1 + \bar{c}_2 \kappa_-) \int_{-1/2}^{1/2} \exp[i\kappa_- d(\frac{1}{2} - \bar{z})] \vartheta(\bar{z}) d\bar{z} \tag{13}$$

with

$$\bar{c}_1 = dqn_f \frac{k_0}{(\kappa_+ - \kappa_-)} [1 - 2R\sin\gamma]/2, \quad \bar{c}_2 = dk_0 \frac{R^{-1}}{(\kappa_+ - \kappa_-)} [R \sin\gamma]/2. \tag{14}$$

Here we have changed to dimensionless units $\bar{z} = z/d$. According to Eq. (13) H_1 appears as a certain weighted average over the director profile $\vartheta(z)$. Note that the contribution $\propto \bar{c}_2$ originates from a partial integration of the $\partial_z \vartheta$ term contained in $Inh(z)$.

Inserting our representation for decaying director profile given in Eq. (2) into Eq. (13), all integrals can be performed analytically and H_1 appears in a natural way as a sum of the contributions of the different eigenmodes $N_k(z)$. Thus eventually the fringe intensity I_{-1} is given as:

$$I_{-1} = \theta_m^2 C_q \, |\sum_{k=1}^{\infty} c_k^{opt} w_k \exp(-\mu_k t)|^2 \tag{15}$$

where the q dependent pre-factor

$$C_q = |(\bar{c}_1 + \bar{c}_2\kappa_-)|^2 \tag{16}$$

and the coefficient

$$c_k^{opt}(q) = \int_{-1/2}^{1/2} \exp[i\kappa_-(q)d(\frac{1}{2} - \bar{z})]N_k(\bar{z}, q)d\bar{z}. \tag{17}$$

capture the diffracting efficiency of a given decay mode.

In Fig. 4 we show some coefficients $c_k^{opt}(q)$ as a function of q'^2. While c_1^{opt} decreases with increasing q'^2, the coefficients c_k^{opt} for $k > 1$ show a damped oscillation in the experimentally relevant q range. In analogy to the maxima of the weights $|w_k|$ (see Fig. 3a) the leading maxima of $|c_k^{opt}|$ are continuously shifting toward higher q'^2 values and appear roughly at the same q' interval with $k = \hat{k}(q')$ as defined for $|w_k(q)|$ in Sect. III. Thus via their product in Eq. (15) the mode selection mechanism (w_k) and the optical efficiency (c_k^{opt}) enhance each other. The product $|w_k(q)c_k^{opt}(q)|$ is shown in Figs. 5a and 5b as a function of q'^2, which is indeed maximal for $k = \hat{k}(q)$. Consequently it is obvious that the initial stage of the pattern decay, at small t, is for a given q governed by the decay rate $\mu_{\hat{k}}(q)$. Since $\hat{k}(q) > 1$ for $q^2 > 4$ we would like to emphasize that the initial decay is not automatically governed by the smallest decay rate $\mu_1(q)$, as one might have guessed intuitively. With increasing t, however, we inevitably arrive at a time t_1 where the relation:

$$|c_{\hat{k}}^{opt} w_{\hat{k}}| exp(-\mu_{\hat{k}} t_1) = |c_{\hat{k}-1}^{opt} w_{\hat{k}-1}| exp(-\mu_{\hat{k}-1} t_1) \tag{18}$$

holds and $\mu_{\hat{k}}-1$ comes into play. Upon further increasing t we will visit all lower k values until $k = 1$ is reached. With the analytical expression (15) at hand there is no difficulty to study the time dependence of $I_{-1}(t)$ in any detail. On the other hand, when only experimental values for $I_{-1}(t)$ are given, we are faced with the problem to extract the decay rates $\mu_k(q)$ in a controlled way. For that purpose we fit the data available in the interval $t_a < t < t_a + T_f$ to an exponential curve $Aexp(-2\mu_f t)$, where the factor 2 in the exponent is obvious since the intensity depends quadratically on the tilt angle (see Eq. (15)). The interval T_f has to be chosen small enough, to allow for discriminating the sequence of the μ_k to be expected with increasing t_a according to our general analysis above. As a test we applied the fitting procedure to the analytical expression for $I_{-1}(t)$ given in Eq. (15). The weights of the decay modes have been calculated from the initial EC state for a number of q values

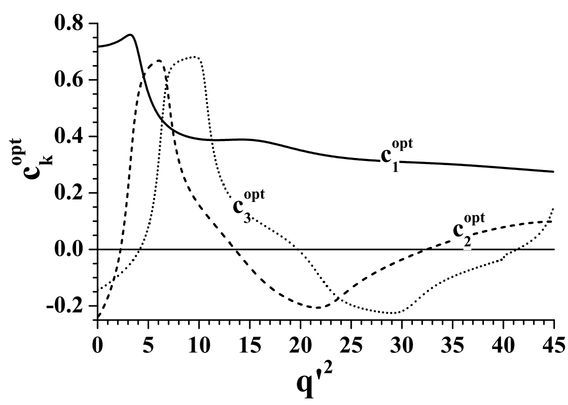

FIG. 4: Variation of the diffraction efficiency of the first (c_1^{opt}, solid line), the second (c_2^{opt}, dashed line) and the third (c_3^{opt}, dotted line) decay eigenmodes with the dimensionless wavenumber square q'^2.

(including ones from the conductive as well as from the dielectric regime). It is convenient to nondimensionalize the effective exponents using the characteristic director relaxation time $\tau_d = \gamma_1 d^2/K_1\pi^2$ (γ_1 is a rotational viscosity, K_1 the splay elastic constant), which is of the order of $1s$ for $d = 10\mu m$. The resulting $\mu'_f = \mu_f\tau_d$ are shown in Fig. 6 together with the first few $\mu'_k = \mu_k\tau_d$ branches as function of q'^2. It is reassuring that our μ'_f reproduce the $\mu'_k = \mu_k\tau_d$ branches very well: the μ'_f follow the μ'_k branches, and exploit their steep parts to switch to higher k values with increasing q'^2. The same scenario has also been observed and discussed before when analyzing the experimental data in [2].

In order to have a closer look at the time dependence of the $I_{-1}(t)$ curves the starting point t_a of our fitting regime was continuously shifted towards larger times. Thus we obtain an effective decay rate $\mu'_f(t_a)$. Figures 7a and 7b exhibit examples of $\mu'_f(t_a)$ for the conductive ($q'^2 = 5.619$) as well as for the dielectric ($q'^2 = 18.796$) regime, respectively. It is seen that the decay rate varies with increasing t_a; a gradual crossover from the decay rate of the dominant mode ($\mu'_f(0) = \mu'_{\hat{k}}$) via the intermediate $\mu'_k(q)$ with $k < \hat{k}$ toward the slowest decay rate μ'_1 is observed.

To allow an easier comparison of the time evolution of $\mu'_f(t_a)$ at various wavenumbers, Fig. 8 contains their values scaled by the largest one, i.e. $\mu'_f(t_a)/\mu'_f(0)$. For the lowest q the slowest mode $\mu_1(q)$ is the dominant one, so $\mu'_f(t_a)$ is practically constant, while for increasing q, where $\hat{k}(q) > 1$ also larger μ_k with $k < \hat{k}$ come into play before the curves

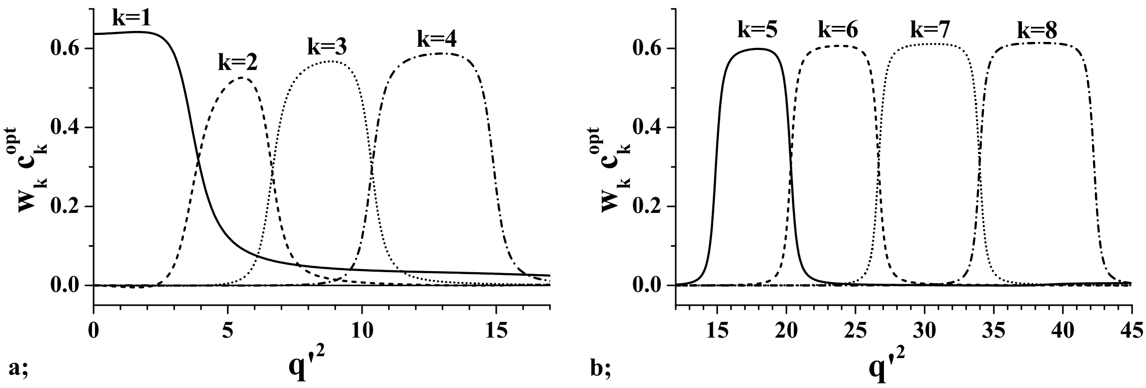

FIG. 5: Contribution of modes to the diffraction intensity $w_k c_k^{opt}$ (plotted with different line styles) with respect to the dimensionless wavenumber square q'^2 for a; $k = 1, ..., 4$ and for b; $k = 5, ..., 8$, assuming a $sin(\frac{\pi}{d}(z + d/2))$ initial director profile.

saturate again at the slowest mode μ_1 at $t_a \gtrsim 15/\mu'_{\hat{k}}$. Notice, however, that by this time, the fringe intensity has already decreased by a factor of $3 \cdot 10^{-7}$ which is much too low to be resolved in the experiment.

For completeness we have also plotted the mode independent normalization factor $|C_q|$ as a function of q'^2 in Fig. 9, which determines the absolute intensity I_{-1} of the first order fringe $n = -1$. It becomes fairly small at large q^2 and approaches zero at a certain γ-dependent wavenumber q_γ. The absolute intensity, which sets a limitation on resolving the patterns, has otherwise no direct relevance for the determination of the decay rates. In addition we have no real access to the initial amplitude θ_m in Eq. (15) which determines the fringe intensity as well.

V. COMPARISON WITH EXPERIMENTS

To compare experiments directly with theory we have at first analysed the decay of initial small-amplitude roll patterns, that have been prepared with applied voltages slightly above the threshold $U_c(\omega)$. In this case for each q the maximal decay rate μ_k with $k = \hat{k}(q)$ could easily be identified. The experimental decay rates μ_{exp} in Fig. 11 agree very well with the theoretical results in Fig. 6 as has been already emphasized in [2].

However, since the pattern amplitude becomes too small at a later stage of the decay

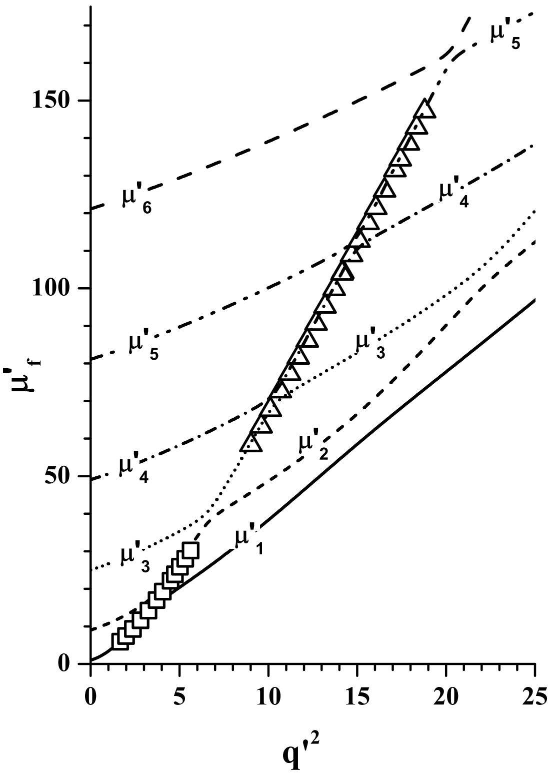

FIG. 6: Dimensionless decay rates μ'_f obtained by a single exponential fit versus q'^2 for the start of the decay. Squares and triangles indicate decay of conductive and dielectric rolls, respectively. The lines of different style depict the $\mu'_1, ..., \mu'_7$ branches of the dispersion relation.

process, it was not possible to reach the further μ_k with $k < \hat{k}$ which must in principle show up (see Fig. 7). Thus we will explore in the following subsections the possibility to initiate the decay process with higher amplitudes and thus to modify the initial conditions.

A. Sine wave excitation

Low amplitude initial patterns are typically produced in our experiments by increasing the applied voltage U slowly above the threshold U_c and waiting some time (of the order of minutes) to allow for equilibration. There is, however, an obstacle to proceed to higher and higher amplitudes θ_m: roll patterns become zigzag unstable already very near to threshold ($\varepsilon \approx 0.04$ [5]). This instability leads to roll pinching, generation of dislocation pairs and thus to defect turbulence, which destroys the homogeneity of the pattern. The resulting

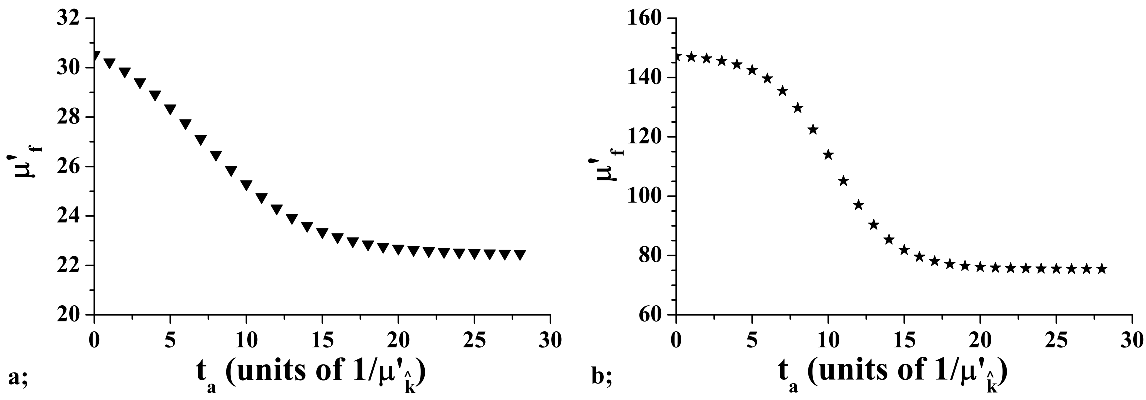

FIG. 7: Dimensionless decay rates μ'_f obtained by a single exponential fit versus the time t_a elapsed between switching off the voltage and start of the fit a; in the conductive regime ($q'^2 = 5.62$, $\mu'_{\hat{k}} = \mu'_2 = 31.28$, $\mu'_1 = 22.42$), b; in the dielectric regime ($q'^2 = 18.80$, $\mu'_{\hat{k}} = \mu'_5 = 147.64$, $\mu'_4 = 121.23$, $\mu'_3 = 94.27$, $\mu'_2 = 84.10$, $\mu'_1 = 73.21$).

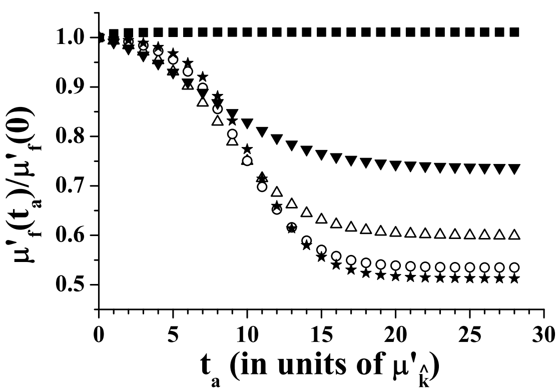

FIG. 8: Temporal evolution of the normalized decay rates $\mu'_f(t)/\mu'_f(0)$ obtained by a single exponential fit for $q'^2 = 1.88$ (solid squares), $q'^2 = 5.62$ (solid up triangles), $q'^2 = 9.02$ (open up triangles), $q'^2 = 15.10$ (open circles) and $q'^2 = 18.80$ (solid stars).

diffuse scattering deteriorates the resolution of diffraction spots and does in practice not allow precise measurements for $\varepsilon \gtrsim 0.07$.

Though the growth of the pattern amplitude and the nucleation of defects are both consequences of driving at higher ε, the two phenomena do not occur on the same time scale. Defects cause a quite extended distortion of the director and of the flow patterns by phase diffusion, thus the characteristic time for this process is typically longer than

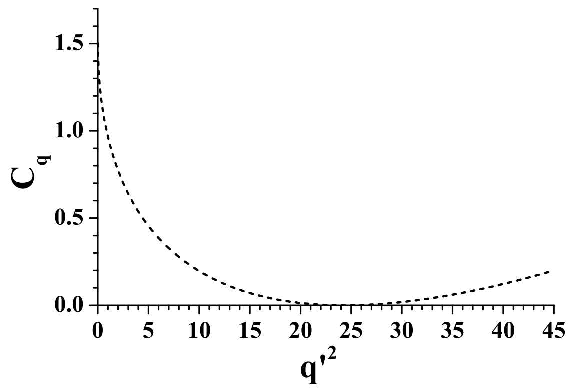

FIG. 9: Variation of C_q with respect to the dimensionless wavenumber square q'^2.

that for the simple growth of the amplitude. Therefore, if we just 'kick' the system by applying a higher voltage for a sufficiently small period only, one expects that the system can be driven temporarily above the zigzag destabilization curve to obtain higher pattern amplitude without the appearance of defects and/or the change of q. Thus we have designed an additional device which has allowed for a fast non-adiabatic amplification of the voltage over a controlled switching period of time $\Delta t_s = 0 - 1$ s. This technique proved to be indeed efficient, as increasing the voltage by 7.5 % (i.e. jumping from $\varepsilon = 0.02$ to $\varepsilon_p \approx 0.18$) for $\Delta t_s = 0.2$ s the number of visible diffraction orders n (note that $I_n \propto \theta_m^{2n}$ [10, 18]) could be temporarily doubled without noticeable increase in scattering. We have found that larger jumps in the applied voltage, have to be associated with shorter periods Δt_s, if we intend to avoid nucleation of defects (i.e. to preserve the sharpness of the fringes). The decay curves for different switching times Δt_s are shown in Fig. 10. In contrast to the monotonuous decay for $\Delta t_s = 0$, from which we extract the decay rates $\mu_{\hat{k}}$, the presence of minima and maxima in the $I_{-1}(t)$ curves recorded at larger Δt_s indicate much bigger initial pattern amplitudes θ_m. The detailed analysis of the decay curves at finite Δt_s is outside the scope of the present paper. At larger amplitude θ_m one leaves the linear regime and both amplitude- and phase grating effects of the periodic director modulations have to be considered. According to the literature ([13],[18]) the fringe intensity I_{-1} is then given as

$$I_{-1} \propto \Big[J_1(Q\vartheta_m) \Big]^2, \tag{19}$$

Here Q is a factor depending on the material parameters and the angle of incidence and J_1 denotes the Bessel function of order 1. The oscillatory behavior of J_1 provides a natural

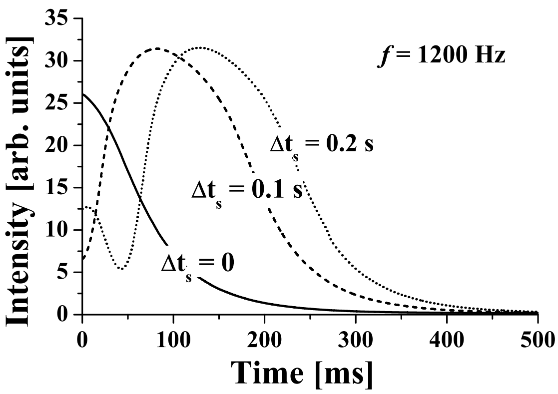

FIG. 10: Temporal evolution of the light intensity of the 1st order diffraction fringe following the shut-down of the applied voltage in a 28 μm thick cell of `Phase 5A`. Curves with different line styles correspond to different values of the period Δt_s during which an increased amplitude excitation ($\varepsilon_p = 0.18$ instead of $\varepsilon = 0.02$) was used.

explanation for the nonmonotonuous Δt_s- dependence of the decay curves. It is clear that with inreasing Δt_s we reach larger θ_m for the same ϵ_p, which is reflected in more oscillations of J_1.

For finite Δt_s it is reasonable to assume, that tails of the $I(t)$ curves in Fig. 10 which monotonously decay in time, will represent the linear θ_m regime which allows to extract the linear decay rate spectrum. It turned out that the resulting μ_{exp} (not shown) were only slightly below the decay rates obtained with $\Delta t_s = 0$.

B. Square wave excitation

The director profile in the EC state is expected to depend also on the driving waveform of the ac voltage. Therefore changing the waveform of the applied voltage from sinusoidal to different ones offers another way to alter the initial conditions.

Thus we have tentatively combined square wave driving with the kicking procedure (a jump from $\varepsilon \approx 0.02$ to $\varepsilon_p \approx 0.18$ for $\Delta t_s = 0.2$ s) described before with the hope to change the initial condition substantially. The decay rates obtained under such conditions are compared in Figs. 11a and 11b with those measured at sinusoidal voltage with $\Delta t_s = 0$. It is seen that in the conductive regime (Fig. 11a) the decay rates obtained by the two types

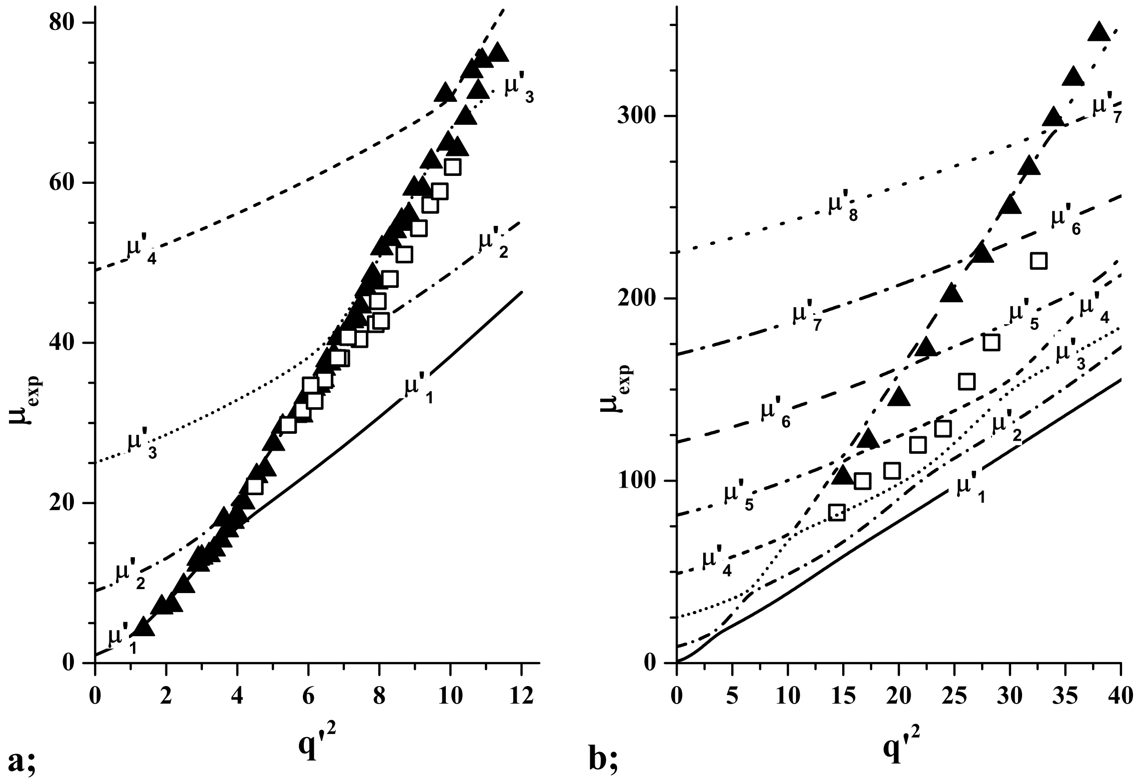

FIG. 11: Theoretical (μ'_k) and measured (μ_{exp}) values of the dimensionless decay rate of the director versus dimensionless q'^2 for a; the conductive mode of `Phase 5A`, b; the dielectric mode of `Phase 5`. Lines of various styles correspond to the eight lowest branches of the dispersion relation. Solid triangles are the data measured at sinusoidal excitation with $\Delta t_s = 0$, empty squares are the data obtained at square wave excitation with $\Delta t_s = 0.2$ s.

of excitation coincide at low q'^2, as expected. The noticeable, though not fully convincing, shift to lower μ_{exp} (slower decay) at higher $q'^2 > 7.3$ may imply that $\mu(k)(q)$ with $k < \hat{k}$ have been activated. Deviations are in particular visible in the dielectric regime (see Fig.11b). There the decay rates follow lower branches μ'_k of the dispersion relation.

At the moment we can only offer some qualitative explanations for this behavior. On the one hand we have passed a highly nonlinear regime (in analogy to Fig. 10), before arriving the decaying branch. Thus it cannot be excluded that the dominant mode with the decay rate $\mu_{\hat{k}}$ has not survived in this process. On the other hand the $z-$profile of the director could also have experienced considerably modifications, such that the product

$c^{opt}_{\hat{k}} w_{\hat{k}}$ is no more the dominant one. To settle the problem we plan to perform nonlinear decay calculations which also allow modifications of the ac waveform.

VI. CONCLUSIONS

In this paper we have presented a rigorous analysis of the decay of stripe (roll) patterns in a planar nematic layer. A precise understanding of the selection process of the dominant mode and its decay rate has been achieved. We found that the dominant decay rate can differ substantially from the slowest one. The results have been applied to a standard nematic (`Phase 5`), where the initial patterns have been generated by electroconvection in the planar configuration. The experimental results are in very good agreement with the quantitative theoretical analysis in the regime of small director distortions, which includes the optical detection of the patterns by diffraction. Some first interesting results for the nonlinear regime and for an ac driving with square waveform need a much more elaborate theoretical analysis, which we plan for the near future.

Acknowledgments

Financial support by the Hungarian Research Grants No. OTKA-T037336, NKFP-128/6, and the EU Research Training Network PHYNECS and to NATO CRG.LG 973103 is gratefully acknowledged. A.B. and W.P acknowledge support and the hospitality of the Isaac Newton Institute for Mathematical Sciences (Cambridge), where the work has been complete.

---

[1] Á. Buka and L. Kramer Eds., *Pattern Formation in Liquid Crystals*, (Springer-Verlag, New York, 1996).

[2] N. Éber, S. A. Rozanski, Sz. Németh, Á. Buka, W. Pesch, and L. Kramer, Phys. Rev. E **70**, 61706 (2004).

[3] P. G. deGennes, *The Physics of Liquid Crystals*, (Clarendon Press, Oxford, 1974).

[4] S. Chandrasekhar, *Liquid Crystals*, (University Press, Cambridge, 1992).

[5] L. Kramer and W. Pesch, in *Pattern Formation in Liquid Crystals*, edited by Á. Buka and L. Kramer (Springer-Verlag, New York, 1996).

[6] M. Treiber, N. Éber, Á. Buka, and L. Kramer, J. Phys. II France **7**, 649 (1997).

[7] We have used a standard electronic switch and a high voltage amplifier. Besides a harmonic time dependence we have used in some cases square shape excitation synthesized by a function generator PC card.

[8] The intensity I_{-1} was monitored by an optical fiber connected to a photomultiplier working in its linear regime. Its output was fed through a current-to-voltage converter to either a 16-bit A/D converter card (for measurements in the conductive regime) or to a digital oscilloscope (for measurements in the dielectric regime, where higher sampling rate required to make a compromise with 8-bit resolution)

[9] see e.g. E. Plaut and W. Pesch, Phys. Rev. E **59**, 1747 (1999).

[10] H. M. Zenginoglou, and J. A. Kosmopoulos, J. Opt. Soc. Am. A **14**, 669 (1997).

[11] H. M. Zenginoglou, and P. L. Papadopoulos, J. Opt. Soc. Am. A **18**, 573 (2001).

[12] E. Bodenschatz, W. Zimmermann, and L. Kramer, J. Phys. France **49**, 1875 (1988).

[13] H. M. Zenginoglou, and J. A. Kosmopoulos, Appl. Opt. **27**, 3898 (1988).

[14] H. M. Zenginoglou, and J. A. Kosmopoulos, Appl. Opt. **28**, 3516 (1989).

[15] J. A. Kosmopoulos, and H. M. Zenginoglou, Appl. Opt. **26**, 1714 (1987).

[16] P. L. Papadopoulos, H. M. Zenginoglou, and J. A. Kosmopoulos, J. Appl. Phys. **86**, 3042 (1999).

[17] R. A. Rigopoulos, and H. M. Zenginoglou, Mol. Cryst. Liq. Cryst. **35**, 307 (1976).

[18] T. John, U. Behn, and R. Stannarius, Eur. Phys. J. B **35**, 267 (2003).

VII. APPENDIX

In this appendix we sketch briefly the decay of a low-amplitude stripe pattern, which is periodic in the x direction (normal roll), using the linearized equations of nemato-hydrodynamics. The relevant variables are the tilt angle of the director, $\vartheta(x,z,t) \approx n_z(x,z,t) = N_z(z)sin(qx)e^{-\mu t}$, and the components, $v_z(x,z,t) = V_z(z)cos(qx)e^{-\mu t}$ and $v_x(x,z,t) = V_x(z)sin(qx)e^{-\mu t}$, of the velocity field. Eliminating v_x by the incompressibility condition the PDEs governing the decay can be written as [2]:

$$\big[-\mu' + k_{33}q'^2 \;-\; \partial^2_{z'}\big]\gamma_1 q' N_z(z') \\ \qquad - \;[\alpha_2 q'^2 + \alpha_3\partial^2_{z'}]V'_z(z') = 0, \tag{20}$$

$$-[\alpha_2 q'^2 \;+\; \alpha_3\partial^2_{z'}]q'\mu' N_z(z') \\ \qquad - \;[\eta_2\partial^4_{z'} - \eta_r q'^2\partial^2_{z'} + \eta_1 q'^4]V'_z(z') = 0, \tag{21}$$

where the quantities

$$\eta_1 \;=\; (-\alpha_2 + \alpha_4 + \alpha_5)/2\ ; \quad \eta_2 = (\alpha_3 + \alpha_4 + \alpha_6)/2\ ; \\ \eta_r \;=\; \eta_1 + \eta_2 + \alpha_1 \tag{22}$$

denote the effective (Miesowicz) shear viscosities, γ_1 is the rotational viscosity, $k_{33} = K_{33}/K_{11}$ is the ratio of elastic moduli. Here we have switched to dimensionless quantities marked by primes. The unit of length is chosen to be d/π, time is measured in units of the director relaxation time $\tau_d = \frac{\gamma_1 d^2}{K_{11}\pi^2}$. We use realistic rigid boundary conditions, i.e. strong planar anchoring of the director and no slip for the velocities at the bounding plates at $z' = \pm\pi/2$ in dimensionless units:

$$N_z = 0, \quad V'_z = 0, \quad \partial_{z'}V'_z = 0 \qquad \text{at} \qquad z' = \pm\pi/2. \tag{23}$$

Eliminating V'_z and looking for solutions $N_z(z) \propto e^{isz'}$ one arrives at the following dispersion relation:

$$(\alpha_2 q'^2 - \alpha_3 s^2)^2\mu' + \gamma_1(\eta_2 s^4 + \eta_r q'^2 s^2 + \eta_1 q'^4)(K'_{33}q'^2 + s^2 - \mu') = 0. \tag{24}$$

Eq. (24) is cubic in s^2 and has three roots (s_1^2, s_2^2 and s_3^2). Thus the corresponding eigenvector is constructed as a superposition from three modes:

$$N_z(z) = \Sigma_{j=1}^3 A_j G_j \cos(s_j z') \\ V'_z(z) = \Sigma_{j=1}^3 A_j \cos(s_j z') \tag{25}$$

with

$$G_j = \frac{\alpha_2 q'^2 - \alpha_3 s_j^2}{\gamma_1 q'(K'_{33}q'^2 + s_j^2 - \mu')}. \tag{26}$$

The corresponding eigenmodes with odd $z-$symmetry are not relevant, since the initial state is always even in z. The boundary conditions in Eq. (23) single out a discrete eigenvalue spectrum μ_i', with the relevant eigenvectors $N_i(z')$ to be calculated from Eq. (25). These eigenvectors are normalized to have the condition

$$\int_{-\pi/2}^{\pi/2} N_i(z')N_i(z')dz' = 1 \tag{27}$$

fulfilled.

Eqs. (20) and (21) can be symbolically rewritten as:

$$\mathcal{L}\mathbf{W_i} = \mu_i'\mathcal{D}\mathbf{W_i} \tag{28}$$

where $\mathbf{W_i} = (N_i(z'), V_i'(z'))$ is a symbolic vector while $\mathcal{L}$ is a matrix differential operator:

$$\begin{aligned}\mathcal{L}_{11} = \left[K_{33}'q'^2 - \partial_{z'}^2\right]q' \ ; \ \mathcal{L}_{12} = -[\alpha_2 q'^2 + \alpha_3\partial_{z'}^2],\\ \mathcal{L}_{21} = \mathcal{L}_{11}\mathcal{L}_{12} \ ; \ \mathcal{L}_{22} = \mathcal{L}_{12}^2 - \gamma_1[\eta_2\partial_{z'}^4 - \eta_r q'^2\partial_{z'}^2 + \eta_1 q'^4],\end{aligned} \tag{29}$$

and

$$\begin{aligned}\mathcal{D}_{11} = q' \ ; \ \mathcal{D}_{12} = 0,\\ \mathcal{D}_{21} = 0 \ ; \ \mathcal{D}_{22} = 0.\end{aligned} \tag{30}$$

Defining the adjoint operator $\mathcal{L}^+$ (and similarly $\mathcal{D}^+$) by the identity

$$\int_{-\pi/2}^{\pi/2} \mathbf{U}\mathcal{L}\mathbf{W}dz' = \int_{-\pi/2}^{\pi/2} (\mathcal{L}^+\mathbf{U})\mathbf{W}dz' \tag{31}$$

one arrives at the adjoint problem:

$$\mathcal{L}^+\mathbf{U} = \mu'\mathcal{D}^+\mathbf{U} \tag{32}$$

The adjoint operator $\mathcal{L}^+$ can be constructed by partial integration of the left hand side of Eq. (29). It follows that $\mathcal{L}_{ij}^+ = \mathcal{L}_{ji}$ holds if the boundary terms introduced by the integration are forced to disappear with proper choice of the boundary conditions for the adjoint problem:

$$\gamma_1 N_z^+ - \alpha_3\partial_{z'}^2 V_z'^+ = 0, \quad V_z'^+ = 0, \quad \partial_{z'}V_z'^+ = 0 \qquad \text{at} \qquad z' = \pm\pi/2. \tag{33}$$

Trivially $\mathcal{D}^+ = \mathcal{D}$ also holds.

It is now easy to see, that the eigenvalue spectra μ_i' of the adjoint and the direct problem (with eigenvectors $\mathbf{U_i} = (N_i^+(z'), V_i'^+(z'))$ and $\mathbf{W_i}$, respectively), coincide. The normalization of the adjoint eigenvectors is given in Eq. (27):

$$\int_{-\pi/2}^{\pi/2} N_i^+(z') N_i^+(z') dz' = 1. \tag{34}$$

In addition the following orthogonality conditions hold:

$$\int_{-\pi/2}^{\pi/2} \mathbf{U_i} \mathcal{L} \mathbf{W_j} dz' = \delta_{ij} \int_{-\pi/2}^{\pi/2} \mathbf{U_i} \mathcal{L} \mathbf{W_i} dz' \tag{35}$$

Combining Eqs. (31) and (30) one obtains that Eq. (35) is equivalent of Eq. (4) as the velocity drops out, i.e. the director profiles of the adjoint eigenvectors and of the EC initial conditions can be used for determining the weights of the decay modes.